A Practical Guide for the Characterization of Lithium-Ion Battery Internal Impedances in PHM Algorithms

Aramis Pérez[1], Matías Benavides[2], Heraldo Rozas[3], Sebastián Seria[4] and Marcos Orchard[5]

[1,2,3,4,5]*Department of Electrical Engineering, Faculty of Physical and Mathematical Sciences, University of Chile, Santiago, Chile*

aramis.perez@ing.uchile.cl
matias.benavides@ing.uchile.cl
heraldo.rozas@ing.uchile.cl
sebastian.seria@ug.uchile.cl
morchard@ing.uchile.cl

ABSTRACT

This article aims at describing the most important aspects to be considered when using the concept of battery internal impedances in algorithms that focus on characterizing the State-of-Health (SOH) degradation of lithium-ion (Li-ion) batteries. The first part provides a brief literature review that will help the reader to interpret the outcome of typical Li-ion discharge and/or degradation tests. The second part of the paper shows preliminary results for accelerated degradation experiments performed on a Li-ion cell under controlled conditions. Results show changes on electrochemical impedance spectroscopy test that can be linked to battery degradation. This knowledge may be of great value when implementing algorithms aimed at predicting the battery End-of-Life (EoL) in terms of temperature, voltage, and discharge current measurements.

1. INTRODUCTION

Since their invention, batteries have been used in a wide variety of applications that require an autonomous energy source, or just as a backup for normal operation. Regardless of how a battery is used, a typical user in interested mainly on two things: how much energy is available and the Remaining-Useful-Life (RUL) of the battery. These two issues are associated to other two concepts: the State-of Charge (SOC) and the State-of-Health (SOH). SOC can be understood as the amount of energy that a battery can deliver until it reaches its End-of-Discharge (EoD) time; an indicator that is particularly useful to characterize short-term operation. Meanwhile, the SOH is an indicator associated with the long-term cycle life of batteries, since every time a battery is used its RUL decreases.

To understand the operation of Li-ion batteries, different types of models have been proposed; being typically categorized as empirical, electrochemical, multi-physics and molecular/atomist (Daigle & Kulkarni, 2013). The most used ones are electrochemical and empirical models.

Independently of the type of model that is used, it is important to note that their main purpose is to describe either how the battery cell discharges or degrades during the cycle life. All these effects are associated with changes in the battery internal impedance. This impedance appears explicitly in empirical circuit models that can be identified at different moments of the life cycle, making possible to quantify the changes of different parameters. In this regard, it is possible to characterize the circuit model as a transfer function of space-state structures, depending on the final application purpose (i.e., estimation or prognostics).

2. COMPONENTS OF A LI-ION BATTERY

The main components of a battery are: the anode (negative electrode), the cathode (positive electrode) and the electrolyte. During the discharge process of a cell, the anode is the one in charge of providing the electrons causing it to oxidize due to the loss of the electrons. Furthermore, the cathode receives the electrons and becomes reduced due to the gain of electrons. The electrolyte is the substance that divides the anode and the cathode, and it is usually a liquid or a solid with dissolved salts to improve the ionic conductivity (Linden, 1984), and when charging, the flow of electrons is the opposite as when discharging.

Besides identifying the main components of a battery, it is important to understand a few common concepts that are related to the electrochemical processes that take place inside the cell. The first concept is the double layer capacitance. It

consists on an electrical double layer between the electrode and the electrolyte. The double layer forms when the ions from the solution are absorbed on the electrode. Other concepts are associated with internal battery resistances: polarization resistance, charge transfer resistance, and electrolyte resistance. The polarization resistance is the one that can be measured between the electrodes and the electrolyte, and it is a product of chemical processes occurring inside the battery. The charge transfer resistance is related to the chemical reaction that occurs when ions are diffused into the electrolyte. This reaction occurs at a speed that depends on the temperature and concentration of materials. The electrolyte resistance depends on the ionic concentration, temperature and area of where the reactions occur. The last concept that is necessary to understand is the process of diffusion. This process consists of the movement of atoms from a high potential area to a low potential area within the concentration area. One important thing to consider regarding the diffusion is that it is also related to a different type of impedance, known as the Warburg impedance, which is frequency-dependent and can be neglected sometimes (at high frequencies). We will discuss these details further on.

2.1. Type of Li-ion batteries

2.1.1. Lithium Cobalt Oxide ($LiCoO_2$)

The high specific energy of this battery type makes it very popular for mobile phones, notebooks, tablets and digital cameras. The cathode is made of cobalt oxide and the anode of carbon graphite. The main disadvantages are a short useful life, low thermal stability, and limited specific power (Buchman, 2016).

2.1.2. Lithium Manganese Oxide ($LiMn_2O_4$)

The components of this battery form a tridimensional structure that allows a better flow of electrons in the electrodes generating a smaller internal resistance and a better current management (Buchman, 2016).

2.1.3. Lithium Nickel Manganese Cobalt Oxide ($LiNiMnCoO_2$ or NMC)

The NMC Li-ion battery uses a cathode combination of nickel, manganese, and cobalt. Nickel has high specific energy but poor stability, while manganese forms a strong structure but offers a low specific energy; making this combination complementary. These type of batteries have good performance and high specific energy. Also, it has the lowest self-heating rate, making it a good candidate for electric vehicles (Buchman, 2016).

2.1.4. Lithium Iron Phosphate($LiFePO_4$)

This chemistry can withstand high temperatures; hence it is stable in overcharge or short circuit conditions. Among its advantages it is possible to mention the environmental benignity, high temperature capability and potential low-cost synthesis (Buchman, 2016).

2.1.5. Lithium Nickel Cobalt Aluminum Oxide ($LiNiCoAlO_2$)

This battery provides great performance in terms of a long lifetime and high power density. Given this advantage, NCA batteries result as a good candidate for electric powertrains. However, it presents a safety and security risk when used in large quantities, increasing its cost synthesis (Buchman, 2016).

2.1.6. Lithium Titanate ($Li_4Ti_5O_{12}$)

This type of cell has a good electrochemical stability. Main advantages of this cell type are: fast recharge time, high efficiency, and long lifetime. Also, this type of battery is considered to be safer. Furthermore it has a wider operating temperature range (Buchman, 2016).

3. ELECTROCHEMICAL IMPEDANCE SPECTROSCOPY

The electrochemical impedance spectroscopy (EIS) consists of a frequency response analysis of an electrochemical system when submitted at a certain voltage. Usually the results are showed using a Nyquist plot with a negative Y-axis, since most electrochemical systems show a more capacitive behavior. This method is fast, non-destructive and a reliable technique capable of identifying the origin of the degradation process and highlights some aging effects that traditional tests do not recognize (Vetter, Novák, Wagner, Veit, Möller, Besenhard and Hammouche, 2005). Figure 1 shows a typical Nyquist plot obtained through this technique. As proposed by these authors, the plot can be divided in three major areas: high frequencies are associated with an inductive effect caused by the geometry of the cell and porosity of the plates; the intercept with the real axis corresponds for the total value of the ohmic resistances; and the low frequency behavior can be related to the capacitive effects. Furthermore, the authors state that at low frequency ranges, where the graph may show a spike, the semicircle end corresponds to Li^+ cation diffusion in the solid-state phase. This semicircle correspond to the relaxation of charge carriers at the SEI, and the other semicircle is dependent to the electrode potential, modeled by a double-layer capacitance and the charge-transfer resistance.

The Warburg impedance can be seen on a Nyquist plot as a diagonal line with positive slope that starts at low frequencies. This impedance is the result of reactants that tend to separate among each other at low frequencies. Figure 2 shows a Nyquist plot where the Warburg impedance part can be appreciated, between the 0.36 Hz and 5 mHz.

As it was previously mentioned, the Nyquist plot can be approximated through different electric components

according the frequency ranges on which these elements have a major influence. For instance, the high frequencies can be represented through an inductance. The cross by zero on the imaginary axis represents a pure resistance element. Then, a RC-parallel branch is used to model the semicircle present on the plot. Last but not least, the Warburg impedance affects the response at low frequencies.

The adjustment of these circuits allow the transformation of visual information obtained with the Nyquist plots, into parameters that evolve in time as the degradation process becomes more evident. This way it is possible to establish a correlation between parameter changes and battery SOH.

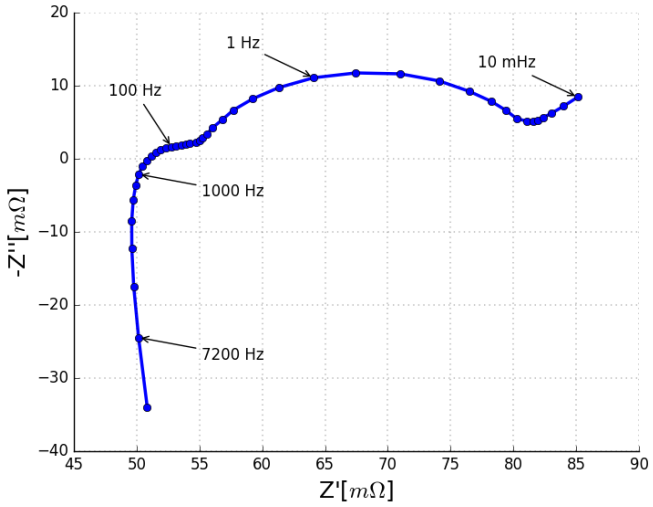

Figure 1. Typical Nyquist plot of a Li-ion battery impedance. Adapted from Vetter et al. (2005).

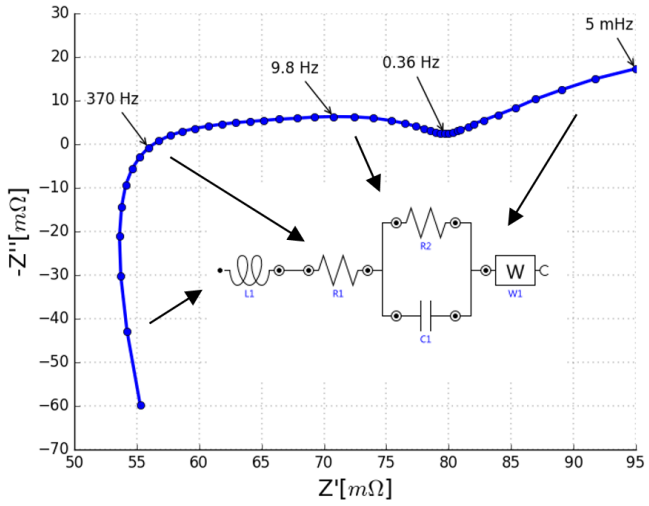

Figure 2. Impedance Nyquist plot and equivalent circuit model. Adapted from Koch and Kuhn (2014).

4. LI-ION BATTERY MODELS

4.1. Electrochemical Models

As the name suggests, these type of models are based on electrochemical equations to represent the effects of discharge or degradation of the batteries. Usually, electrochemical models are very detailed and try to explain the stress that occurs on every component of the inside of the battery. Ning and Popov (2004) propose a capacity fade model that includes the charge rate (CR), the depth of discharge (DOD), the end-of-charge voltage (EOCV) and the discharge rate (DR). In this paper, the authors explain through the use of partial differential equations the flow on ions from the anode to the cathode or vice-versa (depending if the battery is charging or discharging). The changes that occur on the electrodes and electrolyte are the real reasons of why the impedance changes throughout the use.

Similarly, Daigle and Kulkarni (2013) propose a model that describes electrochemical process. The authors propose a set of equations to explain the chemical reactions that occur when the battery is being charged or discharged. Also, the authors establish different types of stress that may affect batteries when operating at low or high temperatures. For instance, at low temperatures the ionic diffusion can be compromised creating a damage such as lithium plating. In case of high temperatures, corrosion and generation of gases can occur, elevating the internal pressure. Also, the authors define four characteristics of the aging effect in the electrodes, which are: solid-electrolyte interface (SEI) layer growth, lithium corrosion, lithium plating and contact loss. The authors emphasize how the loss of mobile ions generate an increase in the internal resistance, which is associated with a rise of the internal temperature of the battery.

Ning, White, and Popov (2006), focus on explaining a charge-discharge model, based on the loss of active Li-ions due to electrochemical reactions that occur at the anode/electrolyte interface. Hence, the rise in the anode film resistance is used to explain the decrease of the discharge voltage as battery ages. In this effort the authors propose that the increased SEI film thickness is related to an increase of the anode film resistance.

It is understood that electrochemical models are accurate but their main disadvantage is the long simulation time that is required (Rong & Pedram, 2003). On this paper, the authors propose two electrochemical reactions that occur at each of the electrodes. Furthermore, the cycle aging is explained as an effect of cell oxidation, electrolyte decomposition, and self-discharge processes. It is important to emphasize that cell oxidation causes a film growth on the electrodes, which causes the internal resistance to rise, and this resistance is proportional to the thickness of the film. This is also supported by Santhanagopalan, Zhang, Kumaresan, and White (2008).

A study of the effects caused by how the different parts of the Li-ion battery degrades according to its use is presented by Vetter et al. (2005). In this paper, the authors propose a detailed analysis of the causes that lead to either capacity or power fade, and how it is enhanced by the different operating conditions. The work presented by these authors also support the findings made all throughout the available literature, perhaps the most important characteristic of this work is the amount of detail presented.

4.2. Empirical Models

Empirical models are built from measured data. Usually, the measured data is fitted in order to obtain an equivalent circuit model. Depending on the approach, the topology of this circuit can change from one study to another.

Figure 3 shows the structure proposed by Wang, He, Sun, Liu, and Wu (2011) as the equivalent model for the internal impedance of a Li-ion battery. In this case, the authors use the following elements: a resistor that represents the resistance of the electrolyte, two branches of a resistor and a capacitor in parallel to represent the negative and positive pole. The branch that includes a resistance and the inductance is aimed to fit the data at high frequencies.

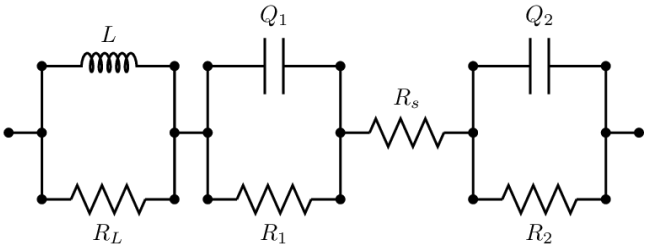

Figure 3. Equivalent circuit model of a battery. Adapted from Wang et al. (2011).

Xie, Lin, Wang, and Pedram (2012) propose a similar model; see Figure 4. In this case the authors state that model is composed by an internal series resistance, and two parallel branches intended to model the internal capacitances.

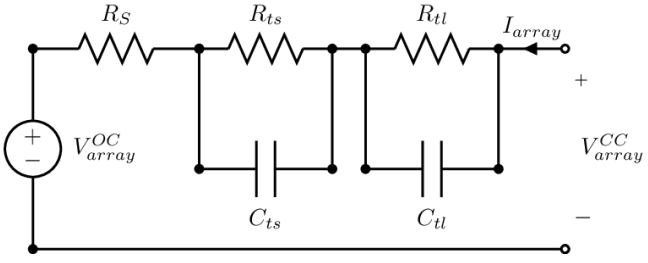

Figure 4. Li-ion battery circuit model. Adapted from Xie et al. (2012).

A semi-empirical proposal is presented by Ramadass, Haran, White, amd Popov (2003). In this case the authors propose a correlation to determine the state of charge and the battery resistance (polarization and film resistance) as a function of the number of cycles. Their approach includes data performance analysis plus a destructive physical analysis of new and cycled electrode materials. In their findings the authors establish that the capacity fade can be separated in three aspects:

- Increase of the resistance on both electrodes.
- Loss of lithiation capacity at the electrodes.
- Loss of active material in the cell.

Zou, Hu, Ma, and Li (2014) present a first-order RC model as the best choice after comparing twelve common equivalent circuit models. This choice is based on complexity, accuracy and robustness, see Figure 5. The model consists of a series resistance and a RC branch intended to represent the diffusion effect.

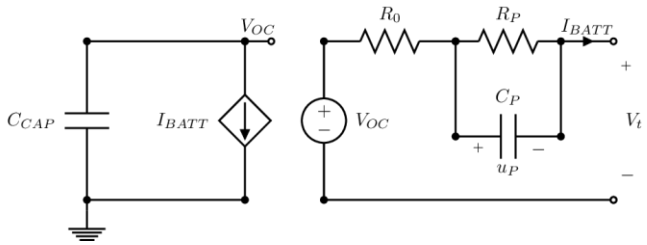

Figure 5. Battery circuit model (the left part explains the SOC, and the right part the voltage-current characteristics). Adapted from Zou et al. (2014).

4.3. Combined Models

Ning, Haran, and Popov (2003) present an interesting approach where a series of analysis is performed to whole-cells and half-cells, using EIS. Also, the authors propose an experimental method to obtain the internal DC resistance of the whole-cells through the use of Ohm's Law. Then, their results are validated with the use of EIS on other cells. One of the major findings in this paper is shown in Figure 6. This figure shows the increase of the internal resistance as a function of the depth of discharge (DOD) after 300 cycles of use. The results were obtained for cells cycled at different currents, and then compared to a brand new cell. It is reported that the value of the resistance by the manufacturer is approximately 200 mΩ, similar to the experimental results. However near the EoD, the value of the resistance tends to increase.

A different way to analyze changes on the battery impedance is using Nyquist plots. In this case, instead of having a DC resistance, an AC impedance can be obtained. This AC impedance is correlated with the actual SOC, so it is very important to know the conditions under which it is measured: when fully charged the impedance of the battery is lower than when the battery is discharged. Also, as reported by the authors, a battery that is cycled at higher currents (2 or 3 times the nominal current) has higher impedance when compared to battery cycled at the nominal current. The authors propose

the use of Croce's model to analyze the EIS results shown in Figure 7. The idea behind this model is that on the Nyquist plots there are three semi-circles that can be noted, depending if the area corresponds to high, medium or low frequencies. High frequencies are associated with the migration of active material through the SEI. At middle frequencies, the semi-circle is associated to the charge-transfer resistance across the interface. Finally, low frequencies, are related to the resistance of the electrode material. Furthermore the slope that can be obtained at low frequencies represents a characteristic associated with the Warburg diffusion region. Additionally, the authors propose an equivalent circuit model that represents the obtained data with the EIS, on Figure 8. For this model, R_{elec} represents the resistance of the active material in the electrolyte. The RC branches are associated respectively to the passivating surface layer, the charge-transfer and the electronic resistance of the material. Also the Warburg impedance is considered as well as a capacitance which effect is only observed at very low frequencies.

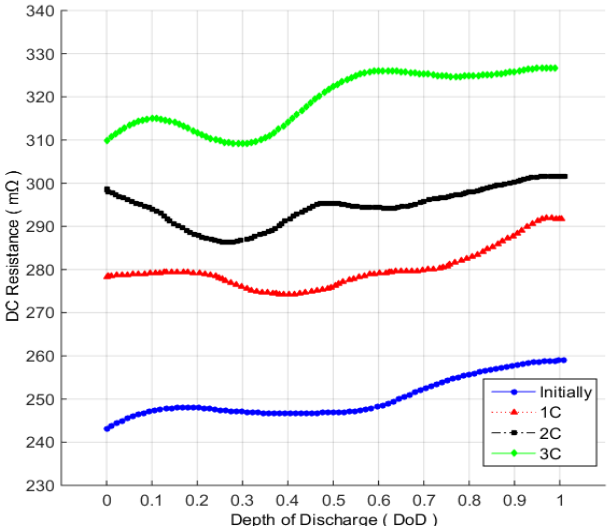

Figure 6. DC Resistance as a function of DOD. Adapted from Ning et al. (2003).

A simpler circuit equivalent model obtained through EIS is presented by Saha, Goebel, Poll, and Christophersen (2009) on Figure 9. In this case C_{DL} represent a double layer capacitance, R_{CT} is the charge transfer resistance, R_W stands for the Warburg impedance and R_E is the electrolyte resistance. In this case the authors also propose the use of a semi-circle on the Nyquist plot in order to find the parameters.

Dai, Wei, and Sun (2009) performed a similar experiment. In thier proposal Li-ion batteries were cycled under different conditions and a variation of the ohmic resistance was obtained. Figure 10 shows how the authors define the evolution of the ohmic and the polarization resistances. The importance of this figure is to note how the polarization resistances is practically constant while the ohmic resistance does change with cycling. Since this resistance tends to increase, the authors, propose to study it in order to understand better the SOH.

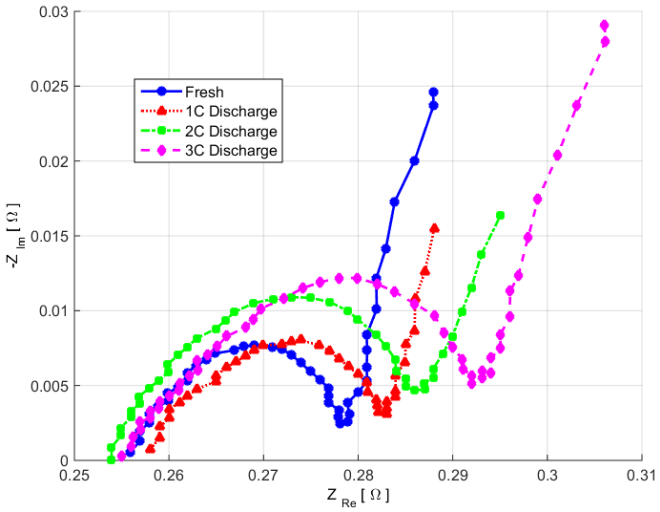

Figure 7. Nyquist plot for a new battery and for used batteries after 300 cycles and 100% SOC. Adapted from Ning et al. (2003).

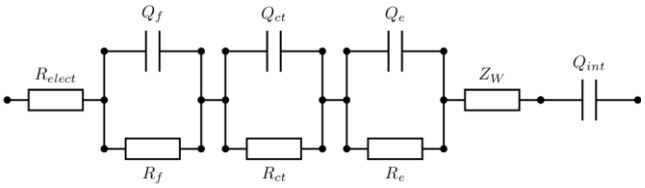

Figure 8. Equivalent circuit model obtained through EIS. Adapted from Ning et al. (2003).

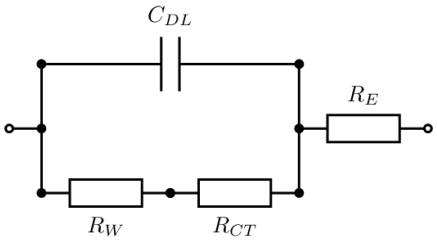

Figure 9. Battery equivalent circuit model. Adapted from Saha et al. (2009).

Figure 11 shows another experiment that was performed. The intention was to measure the ohmic resistance variation (defined as R/R_{new}) when discharged at different multiples of the nominal current and at a temperature of 40 °C. It is easily seen that the resistance increases at higher currents

Since not all cycles are the same, the authors also include the ohmic resistance variation when the battery is discharged at different values of DOD. In this case also, the temperature is 40 °C and the charge and discharge current is equal to the nominal value or 1C. Figure 12 shows the larger DOD cycles have a major impact on the resistance than a more conservative use.

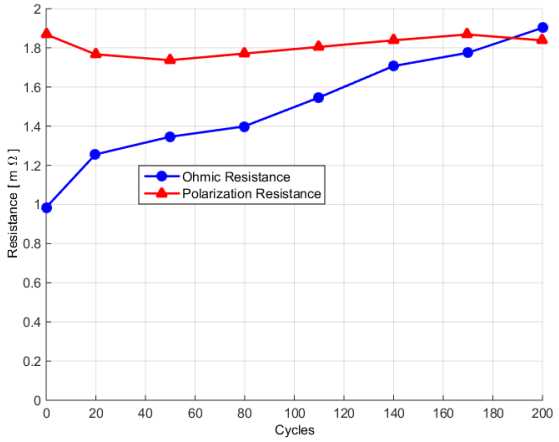

Figure 10. Ohmic and polarizarion resistance. Adapted from Dai et al. (2009).

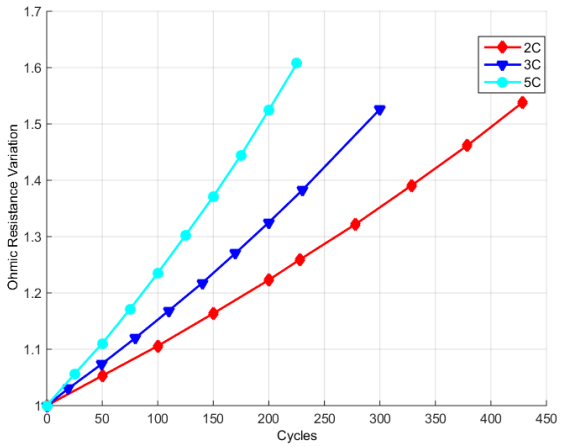

Figure 11. Ohmic resistance variation when cycled at different currents. Adapted from Dai et al. (2009).

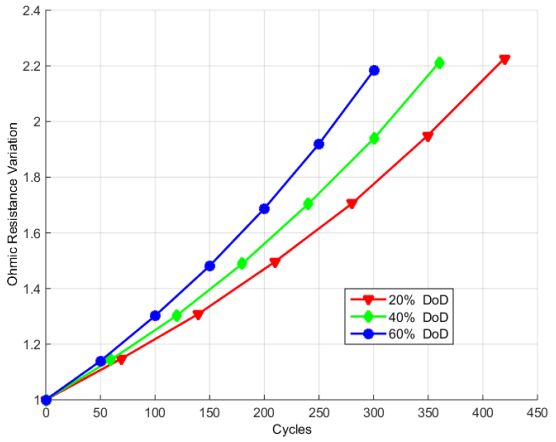

Figure 12. Ohmic resistance variation when cycled at different DODs. Adapted from Dai et al. (2009).

The last result presented by Dai et al. (2009) is an analysis of the ohmic resistance variation, as a function of the temperature when charging and discharging at nominal current. Figure 13 illustrates that the operating temperature has a major impact since the variation trend increases as the temperature is higher.

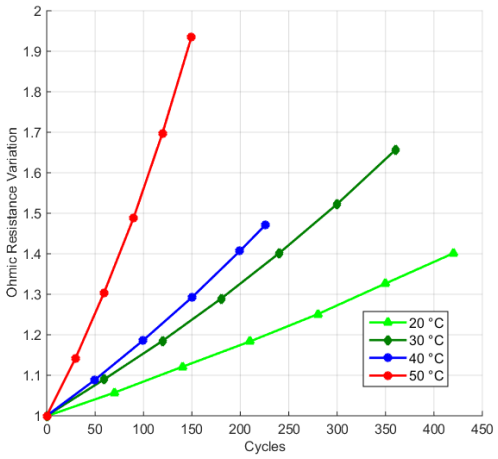

Figure 13. Ohmic resistance variation when cycled at different temperatures. Adapted from Dai et al. (2009).

With these findings, the authors propose the model of Figure 14. The series resistance is used to describe the internal ohmic resistance. The RC branches are used to represent polarization effects, while C_E is a combination of a capacitance and voltage source that depends on the SOC and open circuit voltage.

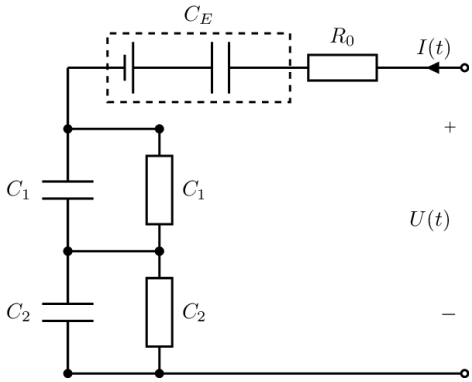

Figure 14. Equivalent circuit model. Adapted from Dai et al. (2009)

5. EXPERIMENTAL TESTS AND OBTAINED RESULTS

The following results aim at illustrating how the degradation process can be studied through the use of EIS and the corresponding Nyquist plots that are generated by this method. Measured data is used to fit two empirical models; one of them offering a more complex structure and, therefore, more parameters. Also, with the Nyquist plots it is possible to determine how the internal impedance varies through cycling, creating a map between the curve and the ohmic

resistance value. This concept was experimentally validated using data from continuous cycling test on Panasonic CGR18650CG Li-ion battery cells (nominal capacity 2250 mAh, and a cut-off voltage of 3 V). The charging protocol forced constant current-constant voltage (CCCV) stages, and the temperature was controlled at 25 °C.

The first 10 cycles were executed at nominal current to allow a proper electrochemical stabilization of the battery. Afterwards, EIS was performed every 20 cycles, when the battery was fully charged, and at 25 °C. The galvanostatic mode was set on, the current amplitude was 50 mA, and the frequency range was between 10 kHz and 5 mHz, with 7 seven measurements per decade.

Figure 15 shows different Nyquist plots obtained throughout the cycling procedure. The initial state curve shows the brand new cell completely charged before any discharge. The other curves show the different Nyquist plots every 100 cycles. It can be observed that the curve displaces to the right on the real axis, until it reaches a point at cycle 480, where the capacity of the battery reaches an 80% of its original value, at nominal current.

Figure 16 shows how the ohmic resistance varies through the cycling experiment. This value is obtained at 370 Hz, which corresponds to the cross by zero on the imaginary axis. At the beginning of the experiment, the value of the experiment is bounded and has small variations, but as the amount of cycles increases, the changes on the resistance also increases. Even more, it is possible to see a major increase on the resistance after 450 cycles. At this point the nominal capacity of the battery is near an 80% of its original value.

Using the experimental data, we are going to focus on three measured cases. Using the measurements we are going to fit the Nyquist plot and generate the equivalent empirical circuit model. The intention is to study the changes on the circuit parameters to determine which of them have a significant variance, when compared to the initial values of the cell prior to start the cycling experiment. In this approach we are presenting two empirical models for comparison purposes. We are focusing on three specific cycles: cycle 0 (new battery), cycle 310 (manufacturer reports information up to cycle 300) and cycle 480 (almost an additional 50% cycles). The value of the ohmic resistance for these cycles are: $R_0 = 52.7\ m\Omega, R_{310} = 54.6\ m\Omega, R_{480} = 56.8\ m\Omega$. Figure 17 shows the Nyquist plot of the measured data and the fitted curve that corresponds to the equivalent circuit shown in Figure 18. In this case, it can be observed that the fitted curve is not very accurate when compared to the measured data. This means that the selection of the particular empirical simple model perhaps might not be a good choice when trying to understand the evolution of the impedance of the battery.

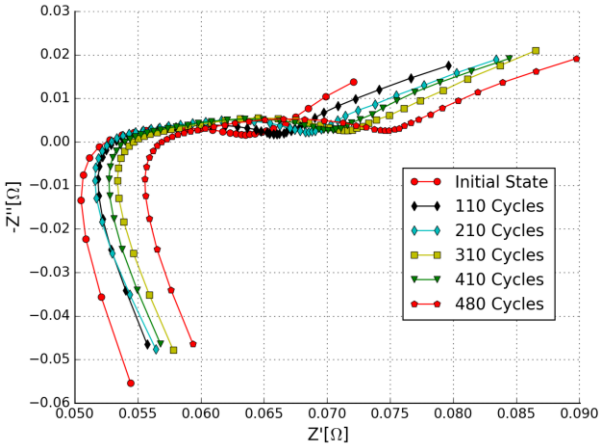

Figure 15. Nyquist plots at different cycles for the performed experiment.

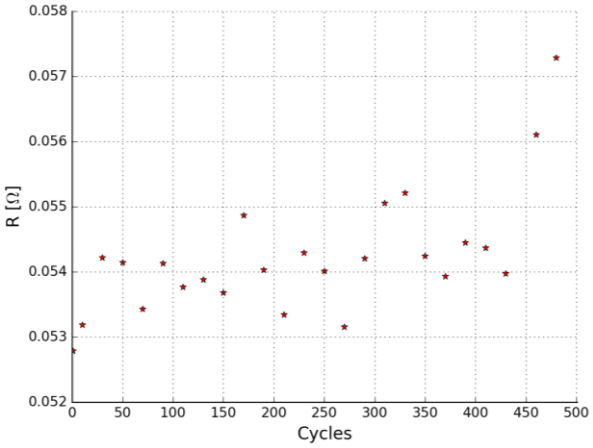

Figure 16. Resistance value at different cycles.

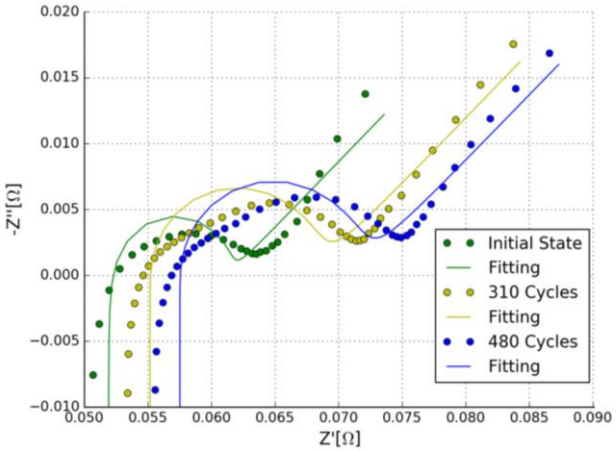

Figure 17. Nyquist plots for measured and fitted data of model #1.

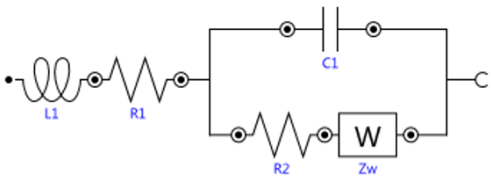

Figure 18. Equivalent empirical circuit model #1.

Table 1 shows the different values of the parameters for the three fitted curves. From the results shown on this table, it is possible to see that the changes on the value of the parameters are considerable. It is important to mention that the value of the R1 resistor, it is very close to the measured ohmic resistance in Figure 16.

Table 1. Circuit parameters for empirical model #1

	Cycle		
	0	310	480
L1 (nH)	883	716	694
R1 (mΩ)	51.9	55.2	57.5
R2 (mΩ)	9.48	13	13.9
C1 (F)	0.245	1.06	1.26
Zw (S)	231	209	212

A second fit was approached using a different model. The Nyquist plot can be seen on Figure 19. In this case, the fitted curve is more accurate when compared to the real data. This means that the empirical model can represent the dynamics of the battery on a better way.

Figure 20, shows the equivalent model obtained for this case. It is important to mention that the two RC branches connected in series with the resistor R3, are equivalent topology that emulates the effect of the Warburg impedance.
Furthermore, Table 2 shows the different values for all the elements for each cycle of operation.

Similar to the previous model, the resistor R1 has a value near the measured value. This means, that regardless of the model, the ohmic resistance is very similar to the actual value.

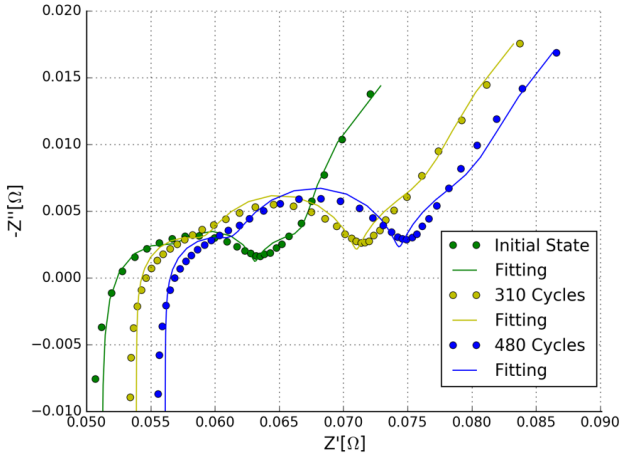

Figure 19. Nyquist plots for measured and fitted data of model #2.

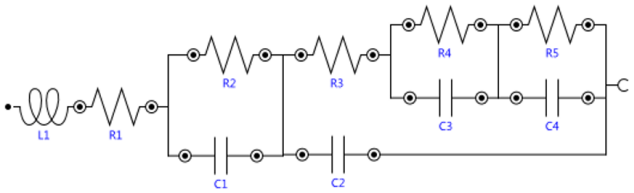

Figure 20. Equivalent empirical circuit model #2.

In this case, Model #2 fits in a better way the measured data, although the variations on the values of the elements is very high except for R2. These models were obtained with the software Nova 2, property of Metrohm Autolab, which allows an option of "Fit and Simulation of equivalent circuit models" through the use of EIS. In this regard, the values of the parameters are optimized to fit the experimental values. Even though the empirical model has many parameters, it is important to keep in mind that each element has a definite contribution on different frequency ranges. If the Nyquist plots are compared it can be seen that model #2, (which has more parameters) fits the real data in a better manner than model #1. Hence, model #2 is able to capture in a better manner the complete range of dynamics of the battery without overfitting the model.

Table 2. Circuit parameters for empirical model #2.

	Cycle		
	0	310	480
L1 (nH)	890	759	738
R1 (mΩ)	51.20	53.90	56.10
R2 (mΩ)	5.71	5.43	5.38
R3 (mΩ)	6.34	11.90	13.00
R4 (mΩ)	3.78	5.92	6.35
R5 (mΩ)	39.70	50.40	49.90
C1 (mF)	124	300	319
C2 (F)	1.68	3.01	3.20
C3 (F)	222	530	579
C4 (F)	954	1200	1270

6. CONCLUSIONS

This paper presents a background on basic terminology associated with Li-ion batteries. Also, the components of this type of batteries is explained, as well as a brief introduction of the different types of resistances that can be located inside the batteries. Even though, sometime the literature refers to Li-ion batteries as a generic product, it is important to know that different chemistries are available on the market, and the purposes of the batteries can be different.

The use of EIS is non-invasive method, very helpful in order to understand the inside of the batteries. Its main disadvantage is the cost of the equipment. However, empirical circuit models are used to represent the dynamics of the batteries. Empirical circuits can be found on the available literature, and some models are more complex than others.

The experimental results, show that first order circuits are too basic when used to explain the equivalent impedance of a Li-ion battery. In our case, a third order model (where the two RC branches that emulate the Warburg impedance are fused into one branch) fits better the measured data. However, some models might neglect this effect since this impedance only affects low frequencies.

Finally, it is important to note that, regardless of the model that is used, the ohmic resistance is generally very close to the value that is directly measured in laboratory tests.

ACKNOWLEDGEMENTS

This work has been partially supported by FONDECYT Chile Grant Nr. 1170044, and the Advanced Center for Electrical and Electronic Engineering, AC3E, Basal Project FB0008, CONICYT. The work of Aramis Perez was supported by the University of Costa Rica (Grant for Doctoral Studies) and CONICYT-PCHA/Doctorado Nacional/2015-21150121.

REFERENCES

Buchman, I. (2016). Batteries in a Portable World: A Handbook on Rechargeable Batteries for Non-Engineers. *Chemistry & …*, (Fourth Edition), 148.

Dai, H., Wei, X., & Sun, Z. (2009). A new SOH prediction concept for the power lithium-ion battery used on HEVs. In *5th IEEE Vehicle Power and Propulsion Conference, VPPC '09* (pp. 1649–1653). IEEE. https://doi.org/10.1109/VPPC.2009.5289654

Daigle, M., & Kulkarni, C. (2013). Electrochemistry-based Battery Modeling for Prognostics. *Annual Conference of the Prognostics and Health Management Society*, 1–13.

Koch, R., & Kuhn, R. (2014). Electrochemical Impedance Spectroscopy for Online Battery Monitoring - Power Electronics Control. In *Power Electronics and Applications (EPE'14-ECCE Europe), 2014 16th European Conference on* (pp. 1–10). IEEE.

Linden, D. (1984). Handbook of batteries and fuel cells. *New York, McGraw-Hill Book Co., 1984, 1075 P. No Individual Items Are Abstracted in This Volume.*, *1*.

Ning, G., Haran, B., & Popov, B. N. (2003). Capacity fade study of lithium-ion batteries cycled at high discharge rates. *Journal of Power Sources*, *117*(1–2), 160–169. https://doi.org/10.1016/S0378-7753(03)00029-6

Ning, G., & Popov, B. N. (2004). Cycle Life Modeling of Lithium-Ion Batteries. *Journal of The Electrochemical Society*, *151*(10), A1584. https://doi.org/10.1149/1.1787631

Ning, G., White, R. E., & Popov, B. N. (2006). A generalized cycle life model of rechargeable Li-ion batteries. *Electrochimica Acta*, *51*(10), 2012–2022. https://doi.org/10.1016/j.electacta.2005.06.033

Ramadass, P., Haran, B., White, R., & Popov, B. N. (2003). Mathematical modeling of the capacity fade of Li-ion cells. *Journal of Power Sources*, *123*(2), 230–240. https://doi.org/10.1016/S0378-7753(03)00531-7

Rong, P., & Pedram, M. (2003). An analytical model for predicting the remaining battery capacity of lithium-ion batteries. *Proceedings -Design, Automation and Test in Europe, DATE*, *14*(5), 1148–1149. https://doi.org/10.1109/DATE.2003.1253775

Saha, B., Goebel, K., Poll, S., & Christophersen, J. (2009). Prognostics Methods for Battery Health Monitoring Using a Bayesian Framework. *IEEE Transactions on Instrumentation and Measurement*, *58*(2), 291–296. https://doi.org/10.1109/TIM.2008.2005965

Santhanagopalan, S., Zhang, Q., Kumaresan, K., & White, R. E. (2008). Parameter Estimation and Life Modeling of Lithium-Ion Cells. *Journal of The Electrochemical Society*, *155*(4), A345. https://doi.org/10.1149/1.2839630

Vetter, J., Novák, P., Wagner, M. R., Veit, C., Möller, K. C., Besenhard, J. O., Hammouche, A. (2005). Ageing mechanisms in lithium-ion batteries. *Journal of Power Sources*, *147*(1–2), 269–281. https://doi.org/10.1016/j.jpowsour.2005.01.006

Wang, H., He, L., Sun, J., Liu, S., & Wu, F. (2011). Study on correlation with SOH and EIS model of Li-ion battery. In *Proceedings of the 6th International Forum on Strategic Technology, IFOST 2011* (Vol. 1, pp. 261–264). IEEE. https://doi.org/10.1109/IFOST.2011.6021018

Xie, Q., Lin, X., Wang, Y., & Pedram, M. (2012). State of health aware charge management in hybrid electrical energy storage systems. In *Design, Automation & Test in Europe Conference & Exhibition (DATE), 2012* (pp. 1060–1065). EDA Consortium. Retrieved from http://dl.acm.org/citation.cfm?id=2492970

Zou, Y., Hu, X., Ma, H., & Li, S. E. (2014). Combined SOC and SOH estimation over lithium-ion battery cell cycle lifespan for Electric vehicles. *Journal of Power Sources*, *273*(January), 793–803. https://doi.org/10.1016/j.jpowsour.2014.09.146

BIOGRAPHIES

M. Sc. Aramis Pérez is a Research Assistant at the Lithium Innovation Center (Santiago, Chile) and Professor at the School of Electrical Engineering at the University of Costa Rica. He received his B.Sc. degree (2002) and Licentiate degree (2005) in Electrical Engineering from the University of Costa Rica. He received his M.Sc. degree in Business

Administration with a General Management Major (2008) from the same university. Currently he is a doctorate student at the Department of Electrical Engineering at the University of Chile under Dr. Marcos E. Orchard supervision. His research interests include parametric/non-parametric modeling, system identification, data analysis, machine learning and manufacturing processes.

Matías Benavides is a graduate student in Electrical Engineering at the Department of Electrical Engineering at the University of Chile, working under the supervision of Dr. Marcos Orchard.

Heraldo Rozas is an undergraduate student at the Department of Electrical Engineering at the University of Chile, working under the supervision of Dr. Marcos Orchard. His research interests include system identification, estimation theory and decision making under uncertainty.

Sebastián Seria is a graduate student in Electrical Engineering at the Department of Electrical Engineering at the University of Chile, working under the supervision of Dr. Marcos Orchard.

Dr. Marcos E. Orchard is Associate Professor with the Department of Electrical Engineering at Universidad de Chile and was part of the Intelligent Control Systems Laboratory at The Georgia Institute of Technology. His current research interest is the design, implementation and testing of real-time frameworks for fault diagnosis and failure prognosis, with applications to battery management systems, mining industry, and finance. His fields of expertise include statistical process monitoring, parametric/non-parametric modeling, and system identification. His research work at the Georgia Institute of Technology was the foundation of novel real-time fault diagnosis and failure prognosis approaches based on particle filtering algorithms. He received his Ph.D. and M.S. degrees from The Georgia Institute of Technology, Atlanta, GA, in 2005 and 2007, respectively. He received his B.S. degree (1999) and a Civil Industrial Engineering degree with Electrical Major (2001) from Catholic University of Chile. Dr. Orchard has published more than 100 papers in his areas of expertise.